Advanced Ceramics Progress: Vol. 11, No. 4, (Autumn 2025) 31-43

Materials and Energy Research Center
MERC

Contents lists available at ACERP

Advanced Ceramics Progress

Journal Homepage: www.acerp.ir

Original Research Article

Effect of Thermal Activation of Iranian Bentonite on Nickel Adsorption Properties from Synthetic Wastewater by Chitosan/Bentonite Composite

Amirmohammad Naghizadeh [a, *], Majid Hosseinzadeh [b], Hamidreza Rezaei [c]

[a] *MS Student, Department of Civil Engineering, Iran University of Science and Technology, Tehran, Iran.*
[b] *Assistant Professor, Department of Civil Engineering, Iran University of Science and Technology, Tehran, Iran.*
[c] *Professor, Department of Materials and Metallurgical Engineering, Iran University of Science and Technology, Tehran, Iran.*

* Corresponding Author Email: amirmohamad.nz.nz@gmail.com (A. Naghizadeh)

URL: https://www.acerp.ir/article_247440.html

ARTICLE INFO

Article History:

Received 30 April 2026
Revised 07 July 2026
Accepted 14 July 2026

Keywords:

Thermally Activated Bentonite,
Chitosan/Bentonite Composite,
Freundlich Isotherm Model,
Nickel-Chitosan Complex,
Adsorbent Beads

ABSTRACT

Contamination of water by heavy metals and organics is a critical environmental issue, with adsorption being a key remediation strategy. Effective adsorbents include clays, zeolites, and biopolymers like chitosan. Chitosan excels at capturing metal cations, but its performance in acidic media, mechanical strength, and immersion behavior can be enhanced through compositing with other materials, such as bentonite. This study synthesized composite beads from chitosan and thermally activated bentonite. A 1.5% (w/v) chitosan solution in 2% acetic acid was mixed with bentonite suspensions at weight ratios of 3.75%, 7.5%, and 15% (w/v). The mixtures were dropwise introduced into an alkaline NaOH solution (pH 7-8) and solidified for 24 hours. Adsorption performance was evaluated using nickel solutions (40-100 ppm). The composite with a chitosan-to-bentonite ratio of 2:1 (CSB2) demonstrated optimal results, achieving 90.4% nickel removal and a capacity of 18.42 mg/g at an initial Ni^{2+} concentration of 80 ppm. This represents a 6.9% improvement in removal efficiency and an 8.9% increase in capacity compared to pure chitosan beads. Fourier-transform infrared spectroscopy (FTIR) confirmed the formation of $Ni(RNH_2)_2^{+}$ complexes within the beads. Adsorption isotherm analysis indicated that the Freundlich and Temkin models best fit the experimental data. Freundlich parameters (Kf = 1.77 mg/L, 1/n = 0.909) confirmed multilayer adsorption on heterogeneous sites with linearly decreasing energy as adsorbate thickness increased. This composite shows enhanced potential for efficient nickel removal from wastewater.

https://doi.org/10.30501/acp.2026.580021.1191

1. INTRODUCTION

The shortage of accessible freshwater resources and widespread contamination caused by industrial, agricultural, and urban activities have become some of the most serious global environmental challenges ("Institute of Standards and Industrial Research of Iran," 1990). ThThe presence of heavy metals such as nickel and organic dyes in industrial wastewater poses significant problems both for reuse and for discharge into the natural environment and groundwater. Nickel enters wastewater mainly from metal electroplating plants, battery manufacturing, paint production, and related industries. The nickel ion concentration in such effluents generally ranges from 50 to 100 ppm, which can cause severe toxic effects on human and animal health. The

Please cite this article as: Naghizadeh, A. , Hosseinzadeh, M. , & Rezaei, H. (2025). Effect of Thermal Activation of Iranian Bentonite on Nickel Adsorption Properties from Synthetic Wastewater by Chitosan/Bentonite Composite. *Advanced Ceramics Progress*, *11*(4), 31-43. https://doi.org/10.30501/acp.2026.580021.1191

permissible limits for nickel are 0.2 ppm in agricultural water, below 1 ppm in effluents discharged into the environment, and 0.7 ppm in drinking water. Achieving these levels often requires multistage wastewater treatment (Pirilä, 2015; Wang & Chen, 2014).

Among various treatment methods, adsorption is one of the most effective techniques for controlling nickel concentrations in wastewater. In this process, nickel ions bind to solid surfaces containing active functional groups. Such binding can occur physically via van der Waals forces or chemically via ionic and covalent bonds (Aliku, 2017). Adsorbents may include clays, zeolites, agricultural wastes, industrial by-products such as microsilica, bio-adsorbents such as algae, different forms of carbon, and various hydrogels such as chitosan or its composites (Al-Nuaim et al., 2023). One of the most widely studied composites is chitosan/bentonite, which has been employed to overcome the limitations of chitosan, such as low acid resistance, insufficient mechanical strength, and limited adsorption of certain metal cations (El-Baz et al., 2020; Salimi et al., 2025; Teofilović et al., 2014).

Chitosan, derived from the skeletons of mollusks, insects, and certain mushrooms, is crystalline, hydrophilic, and contains functional amino ($–NH_2$) and hydroxyl (–OH) groups that provide active adsorption sites for pollutants (Alemu et al., 2023; Eser et al., 2012). Bentonite is a clay mineral consisting mainly of layered montmorillonite along with impurities such as quartz and cristobalite. Montmorillonite possesses negatively charged surfaces and exchangeable cations (e.g., Na^+ and Ca^{2+}), which make it highly suitable for pollutant adsorption (Bahranowski et al., 2021; Hodžić et al., 2020; Zhu et al., 2016). In addition, bentonite exhibits good acid resistance, enhances the mechanical strength of chitosan, and helps overcome chitosan's low density and flotation problems in aqueous media. Both chitosan and bentonite are environmentally friendly, biocompatible, and can be regenerated and reused.

To improve the adsorption efficiency of bentonite, thermal and chemical activation techniques are often applied. Thermal activation involves calcination at around 400-500 °C, which removes interlayer water molecules and creates additional space for chitosan intercalation during composite formation, as well as for pollutant cation uptake (Alemu et al., 2023). Chemical activation is carried out either under alkaline or acidic conditions. In alkaline activation, bentonite is treated with solutions such as calcium carbonate, while in acidic activation, strong acids such as hydrochloric acid are used. Acid activation enhances the specific surface area of bentonite, increases diffusion pathways, and consequently improves its adsorption performance (Tirtom et al., 2012).

Giannakas et al. (Giannakas & Pissanou, 2018) prepared chitosan/bentonite composites by separately dissolving chitosan in acetic acid and dispersing bentonite in water, followed by mixing the two suspensions. After pH adjustment, the suspension was added dropwise into an alkaline solution containing $CaCl_2$ (or other alkalis) to form millimeter-sized composite beads. In the resulting composite, part of the chitosan intercalated between montmorillonite layers, while the remainder surrounded bentonite particles. They reported that these composite beads achieved about 88% nickel removal and an adsorption capacity of 10 mg/g at an initial Ni cation concentration of 200 mg/L (Giannakas & Pissanou, 2018). To further enhance adsorption, various modifications, such as cross-linking of chitosan molecules using agents like formaldehyde and glutaraldehyde, have been investigated (Bahranowski et al., 2021).

Buscano et al. (Buscano et al., 2009) studied cross-linked chitosan/montmorillonite composites for the adsorption of heavy metal ions from aqueous media. Their results showed that both Langmuir and Freundlich isotherm models provided a good fit to the experimental data.

The present study aims to investigate the use of thermally activated Iranian bentonite for improving the properties of chitosan/bentonite beads in nickel adsorption from wastewater, with a particular focus on microstructural characterization and isotherm modeling.

2. MATERIALS AND METHODS

Medium-molecular-weight chitosan was purchased from Iran Sabz Gostar Company, and Iranian bentonite from Semnan Province was supplied by Iran Barite Company as the main raw materials for preparing the composite beads. Acetic acid (Sigma-Aldrich) was used for dissolving chitosan, nickel sulfate hexahydrate for preparing pollutant solutions of various concentrations, NaOH for preparing the alkaline coagulating solution, and a 25% ammonia solution (Dr. Mojallali Co.) for pH adjustment.

For thermal activation, bentonite was heated at a rate of 5 °C/min to 400 °C and maintained in an Azar Iran electric furnace for 3 h, followed by cooling inside the switched-off furnace. Simultaneous thermal analysis (STA), including differential thermal analysis (DTA) and thermogravimetric analysis (TGA), was employed to investigate the changes occurring during calcination.

The preparation procedure of the chitosan/bentonite composites is illustrated in Fig. 1. First, 15 g of chitosan was dissolved in 100 cc of a 2% acetic acid solution and stirred using a Labincol-73 magnetic stirrer at 200 rpm and 50 °C for 4 h, followed by continuous stirring for an additional 6 h at room temperature. Separately, bentonite powder with a particle size below 53 µm was dispersed in 100 cc of deionized water at amounts of 0.375, 0.75, and 1.5 g to prepare suspensions, each stirred for 30 min. To produce composites with different chitosan-to-bentonite weight ratios of 4:1, 2:1, and 1:1, the prepared

bentonite suspensions were gradually added to the chitosan solution and stirred at room temperature for 6 h. The obtained chitosan/bentonite suspensions were then allowed to stand for 12 h to improve homogeneity, stirred again for 1 h, and subsequently added dropwise using a decanter into 250 cc of an aqueous solution containing 20 g NaOH (pH = 8). The mixture was maintained for 24 h to complete bead formation. Finally, the composite beads were separated by filtration, washed with deionized water, and dried in an oven at 60 °C.

The appearance of the chitosan/bentonite beads formed in the alkaline solution is shown in Fig. 2.

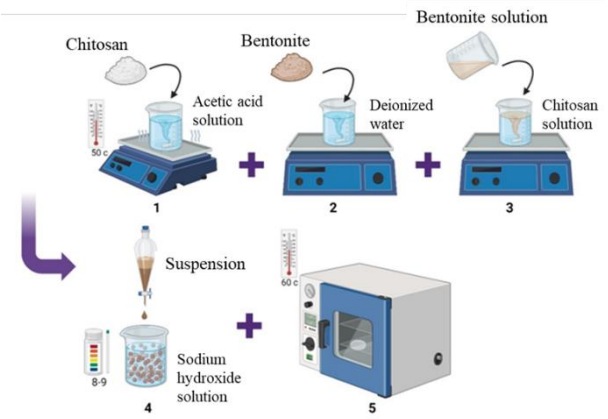

Figure 1. Preparation procedure of chitosan/bentonite composite

Figure 2. Formation stage of chitosan/bentonite composite beads in NaOH solution

In addition to the chitosan/bentonite composite beads, pure chitosan beads were also prepared using the same procedure without the addition of bentonite suspension. The studied formulations and their corresponding codes are presented in Table 1.

TABLE 1. Different formulations of the investigated beads

Code	Chitosan-to-thermally activated bentonite weight ratio
CS	Without bentonite
CSB1	1:1
CSB2	2:1
CSB4	4:1

Nickel-containing pollutant solutions were prepared by dissolving nickel sulfate hexahydrate in double-distilled water, yielding solutions with concentrations of 40, 60, 80, and 100 mg/L (ppm). For the adsorption experiments, 0.2 g of each prepared bead was placed in 50 cc of the different nickel solutions and stirred using a magnetic stirrer at 25 °C for 24 h, with a stirring speed of 100 rpm and the pH adjusted to 7-8. The remaining nickel concentration in the solutions was determined by atomic absorption spectroscopy using a GBC932PLUS instrument.

After drying at 60 °C, the beads were characterized using Fourier-transform infrared spectroscopy (FTIR) with a SPECTRUMRXJ device, X-ray diffraction (XRD) with an XMP-300 instrument, and microstructural analysis using a TESCAN VEGA/XMU scanning electron microscope (SEM).

Following the determination of equilibrium concentrations (the remaining nickel concentration after 24 h) for each bead type, the adsorption percentage and equilibrium adsorption capacity were calculated using Equations 1 and 2 (Gupta et al., 2021).

$$A = \frac{(C_0 - C_e)}{C_0} \times 100 \quad (1)$$

$$q_e = \frac{(C_0 - C_e) \times V}{W} \quad (2)$$

In the above equations, A represents the percentage of pollutant removal; C_0 and C_e are the initial and equilibrium concentrations (mg/L), respectively; W is the mass of adsorbent in grams; and V is the volume of the initial solution in liters.

To elucidate the adsorption mechanism and assess the conformity of the experimental data with adsorption isotherm models, the Langmuir, Freundlich, and Temkin models were employed (Dada et al., 2012). The Langmuir model is based on a fixed number of adsorption sites and monolayer adsorption, and is described by Equation 3.

$$\frac{C_e}{q_e} = \frac{1}{q_m k_L} + \frac{C_e}{q_m} \quad (3)$$

By plotting datas C_e/q_e versus C_e, a straight line should be obtained. The maximum adsorption capacity, q_m

(mg/g), and the Langmuir adsorption equilibrium constant, K_L (L/mg), can be determined from the slope and intercept of the resulting plot, respectively.

The Freundlich model is used to describe adsorption on heterogeneous surfaces and multilayer adsorption, and it is expressed by Equation 4.

$$\ln q_e = \ln K_f + (1/n) \ln C_e \quad (4)$$

By plotting $\ln q_e$ versus $\ln C_e$, a straight line is obtained. The slope of this line corresponds to 1/n, and the intercept corresponds to $\ln K_f$. Here, n is the adsorption intensity constant, and K_f is the Freundlich adsorption capacity constant, where a higher value of K_f indicates a greater adsorption capacity of the adsorbent.

The Temkin model is based on the assumption that the heat of adsorption decreases linearly with the thickness of the adsorbate layer, and it is expressed by Equations 5 and 6.

$$B \ln A + B \ln Ce = qe \quad (5)$$

$$b_T = RT/B \quad (6)$$

The constants B and lnA are obtained from the plot of q_e versus $\ln C_e$. Here, A is the Temkin equilibrium constant (L/g), and B is a constant related to the heat of adsorption. B value greater than one indicates physical adsorption, while a value less than one indicates chemical adsorption. Higher A values represent greater adsorption capacity of the adsorbent, and higher b_T values which are inversely related to B and referred to as the Temkin constant indicate stronger adsorbent-adsorbate interactions (Zia et al., 2019).

3. RESULTS AND DISCUSSION

3.1. The X-ray diffraction patterns of chitosan and activated bentonite

The X-ray diffraction (XRD) patterns of medium molecular weight chitosan powder, natural bentonite, and bentonite after thermal activation at 400 °C in an electric furnace are presented in Fig. 3.

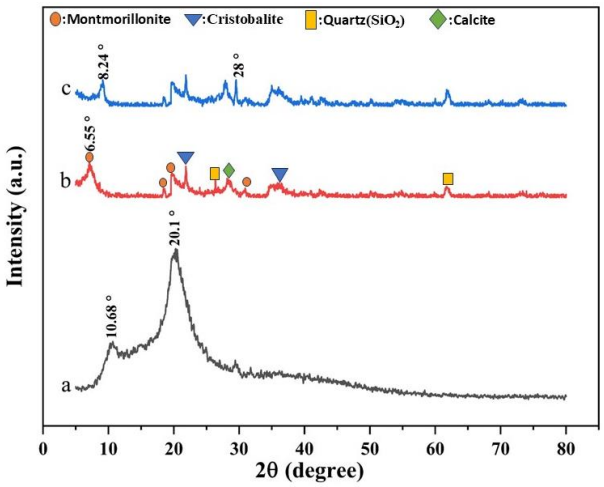

Figure 3. X-ray diffraction (XRD) patterns of (a) chitosan powder, (b) natural bentonite, and (c) thermally activated bentonite.

As shown in Fig. 3(a), the commercial chitosan used is crystalline, with characteristic peaks observed at 2θ = 20.1° and 10.6°. The main peaks correspond to the (001) and (100) planes of the monoclinic chitosan crystal system, with an interplanar spacing of 0.45 Å. These peaks indicate a high degree of deacetylation of chitin during chitosan preparation (Guibal, 2004), which implies a greater number of amino and hydroxyl groups in the chitosan used for the preparation of composite beads, playing a key role in pollutant adsorption. In addition to the deacetylation degree of the initial chitosan powder, factors such as the percentage of mesopores (۲–۵0 nm) and the drying method of pure or composite chitosan beads also significantly influence the adsorptive activity of chitosan (Ahmad et al., 2015).

Fig. 3(b) shows that the natural Iranian bentonite mainly consists of montmorillonite, along with impurities such as cristobalite, quartz, and calcite. The formula of montmorillonite can be expressed as $Ca_{0.15}(Al_{1.7}Mg_{0.3})(Si_4O_{10})(OH)_2 \cdot 4H_2O$, where Ca^{2+} can be partially replaced by Na^+ up to twice the molar amount. The monoclinic crystal structure of montmorillonite consists of tetrahedral SiO_4 sheets and octahedral AlOOH sheets forming a three-layer structure, with two tetrahedral layers sandwiching one octahedral layer. Upon heating below 600 °C, interlayer water molecules are removed and above 600 °C, hydroxyl groups (–OH) from the octahedral sheets are released (do Nascimento, 2021).

As shown in Fig. 3(c), the interlayer spacing of the (001) plane in the C-axis direction for raw Iranian bentonite is 13.4 Å, corresponding to a diffraction angle of 2θ = 6.55°, which can be calculated using Bragg's law (Equation 7) (Wang et al., 2019). In this equation, d is the interplanar spacing, θ is the diffraction angle, and λ is the

X-ray wavelength. The wavelength of the Cu K α line of x-ray diffraction instrument was 1.544 Å.

$$2d.\sin\Theta = n\lambda \quad (7)$$

Characteristic peak of natural bentonite shifted from 2θ = 6.55° to 2θ = 8.24°, and the interlayer spacing of the (001) plane in montmorillonite decreased from 13.4 Å to 10.72 Å. This shift is attributed to the removal of interlayer water molecules during heating, which allows the montmorillonite layers to move closer together due to van der Waals forces.

3.2. DTA/TG analysis of activated bentonite

To investigate the thermal behavior of bentonite during activation, simultaneous differential thermal analysis and thermogravimetric analysis (DTA–TG) were performed, and the resulting curves are shown in Fig. 4.

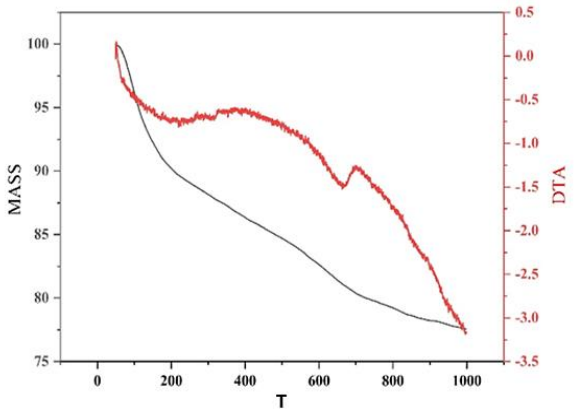

Figure 4. Simultaneous differential thermal analysis and thermogravimetric analysis (DTA+TG) of natural bentonite at a heating rate of 10 °C/min in air atmosphere.

As observed, below 400 °C, a broad endothermic peak accompanied by significant weight loss is detected, corresponding to the removal of interlayer water molecules. Another endothermic peak with associated weight loss around 700 °C is attributed to the release of hydroxyl groups (–OH) from the octahedral AlOOH sheets.

3.3. Investigation of nickel cation adsorption by different beads

To enhance the statistical validity of the adsorption data, all batch experiments were carried out in triplicate under identical conditions, and the results are expressed as the mean values. Table 2 summarizes the equilibrium adsorption capacity (qe) and nickel removal efficiency for chitosan beads (CS) at varying initial nickel concentrations. According to the results, at an initial concentration of 80 ppm, the nickel removal efficiency reached 84.5%, corresponding to an equilibrium adsorption capacity of 16.9 mg/g. The experiments were conducted under constant conditions: temperature of 25°C, contact time of 24 hours, stirring speed of 100 rpm, pH 7–8, and adsorbent dosage of 0.4 g per 100 mL of nickel solution.

TABLE 2. Equilibrium adsorption capacity (q_e) and removal percentage for chitosan beads (CS) at different initial nickel concentrations under fixed temperature, contact time, and adsorbent dosage

Removal percentage (%)	Equilibrium adsorption capacity q_e(mg/g)	Initial nickel concentration (ppm) C_0
83.8	8.4	40
83.2	12.5	60
84.5	16.9	80
81.1	20.3	100

Table 3. Equilibrium adsorption capacity and nickel removal percentage from aqueous solution at an initial Ni concentration of 80 ppm for three chitosan/bentonite composites under fixed conditions: temperature 25 °C, contact time 24 h, stirring speed 100 rpm, pH 7–8, and adsorbent dosage of 0.4 g per 100 mL of solution.

TABLE 3. Equilibrium adsorption capacity (q_e) and removal percentage for Chitosan/Bentonite beads (CSB) at different initial nickel concentrations under fixed temperature, contact time, and adsorbent dosage

Ni removal efficiency (A, %)	Equilibrium adsorption capacity, qe (mg/g)	Adsorbent type
75.1	15.02	CSB1
90.4	18.42	CSB2
84.6	16.92	CSB4

The results in Table 3 indicate that the Ni removal efficiency of the CSB2 composite bead reaches 90.4%, with an equilibrium adsorption capacity of 18.42 mg/g. Compared to the pure chitosan bead under identical conditions, this represents an increase of 6.9% in removal efficiency and 8.9% in adsorption capacity. In the CSB2 composite, the weight ratio of chitosan to bentonite is 2:1. Both chitosan and bentonite are effective adsorbents for nickel ions. The adsorption mechanism in chitosan involves electrostatic attraction and the formation of complexes between nickel ions and amino groups in the form of Ni(-NH_2), as illustrated in Fig. 5. In contrast, the adsorption mechanism in montmorillonite, the main mineral in bentonite, occurs through two pathways: (i) adsorption by the negatively charged surface sites of montmorillonite particles, and (ii) cation exchange of Ni^{2+} with Na^+ and Ca^{2+} ions present on the surfaces or within the interlayers of montmorillonite.

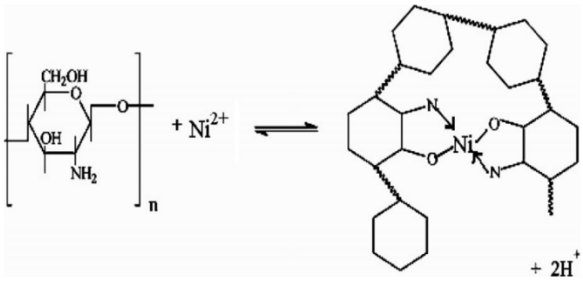

Figure 5. Complex formation between chitosan and nickel ions (Vijaya et al., 2008)

When the bentonite suspension is introduced into the chitosan solution and subsequently dropped into an alkaline medium during bead formation, polymerization of chitosan occurs both within the interlayer spacing of the montmorillonite sheets and around their particles, resulting in the formation of the chitosan/bentonite composite. The deeper the penetration of chitosan into the montmorillonite interlayers, the better the performance of the composite compared to a case in which chitosan is only deposited around the particle surfaces. This is because, in the former case, all three adsorption mechanisms, electrostatic interaction, complexation between nickel ions and amino groups of chitosan, and ion exchange, are activated simultaneously. The contribution of each mechanism, however, depends on other factors such as pH, specific surface area, pore size, and the diffusion pathway of ions from the pollutant-bead interface into and within the bead. A schematic illustration of the chitosan/montmorillonite composite is shown in Fig. 6. Chitosan consists of repeating units of $C_6H_{11}NO_4$ (Alemu et al., 2023).

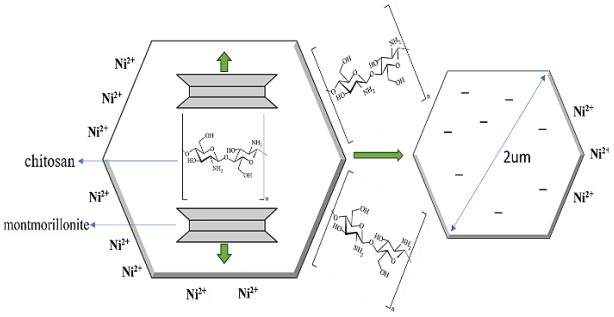

Figure 6. Schematic representation of the arrangement of chitosan within the chitosan/montmorillonite composite and its interaction with the nickel solution

One of the most critical parameters influencing adsorption is the pH of the contaminant solution. To investigate this factor, the effect of solution pH on the adsorption behavior of the CSB2 composite bead in nickel-containing solution was studied. The results are presented in Fig. 7.

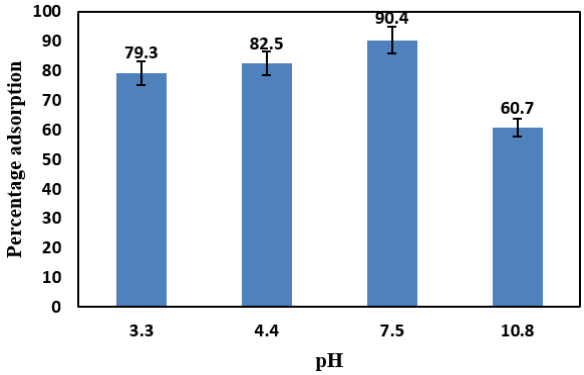

Figure 7. Percentage adsorption of the chitosan/bentonite composite bead (CSB2) at different pH values for a nickel solution with an initial concentration of 80 ppm

As illustrated in Fig. 7, the adsorption efficiency decreases under both acidic and alkaline conditions outside the range of pH ≈ 7.5. At lower pH values, the positive surface charge developed on the composite beads generates electrostatic repulsion, which hinders the adsorption of Ni^{2+} ions onto the adsorbent surface. Conversely, at higher pH values, a portion of the Ni^{2+} ions precipitates in the form of nickel hydroxide [$Ni(OH)_2$], thereby reducing the concentration of free nickel ions available for adsorption and consequently lowering the overall adsorption percentage. Zia et al. (Zia et al., 2019) also reported that at low pH values, the probability of Ni(-NH_2) complex formation decreases, while at higher pH values, the likelihood of complex formation increases.

3.4. FTIR analysis of activated bentonite and bentonite/chitosan composite before and after adsorption

To further investigate the structural changes and the behavior of functional groups during bentonite thermal activation, bead preparation, and subsequent nickel adsorption, Fourier-transform infrared spectroscopy (FTIR) was conducted. The FTIR spectra of natural and calcined bentonite are shown in Fig. 8.

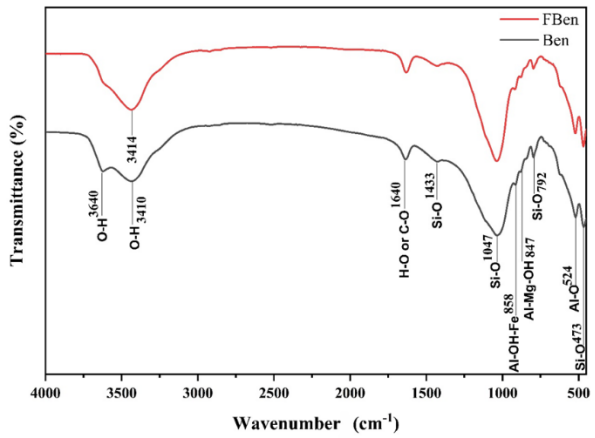

Figure 8. FTIR spectra of raw bentonite (Ben) and thermally activated bentonite at 400 °C (FBen)

The natural bentonite sample consisted mainly of montmorillonite, cristobalite, quartz, and calcium carbonate. Therefore, various characteristic vibrational bands corresponding to Al–O, Al–OH, Si–O, Al–Fe–O, Al–Mg–O, C–O, OH stretching in octahedral layers, and OH stretching of interlayer water molecules are expected to appear in its spectrum. As observed in Fig. 8, these bands were successfully identified at different wavenumbers. The main vibrational frequencies of clay minerals, especially montmorillonite, are summarized in Table 4, which is a combination of text, tables, and figures from the cited sources (Jozanikohan & Abarghooei, 2022; Madejova, 2003; Majiya et al., 2023). Upon thermal activation by calcination at 400 °C, the most significant changes were related to the O–H vibrations. In particular, the band intensity at 3640 cm^{-1} decreased, while the shape of the band around 3410 cm^{-1} also changed slightly. This indicates that, in addition to the removal of a considerable amount of interlayer water molecules, minor changes occurred in the OH groups associated with Al–OH octahedra.

TABLE 4. List of the main vibrational bands of clay minerals, especially montmorillonite (Jozanikohan & Abarghooei, 2022; Madejova, 2003; Majiya et al., 2023)

Wavenumber (cm^{-1})	Vibration type / Assignment
3699	O–H stretching vibration
3650	O–H stretching vibration
3620	O–H stretching vibration
3598	Fe^{3+}…O–H stretching vibration
3400–3640	O–H stretching vibration of interlayer water
1109	Si–O stretching vibration
1033	Si–O–Si stretching vibration
1010	Si–O–Si stretching vibration
937	In-plane Al–OH–Al vibration
915–912	Out-of-plane Al–OH–Al vibration
857	Al–OH–Fe^{3+} vibration
846	Al–Mg–OH vibration
842	Al–Mg–OH vibration
800	Si–O vibration (quartz)
778	Si–O vibration (quartz)
757	Al–OH vibration
700	Al–OH vibration
540	Al–O vibration
471	Si–O vibration
431	Si–O vibration

Fig. 9. FTIR spectra of the chitosan/bentonite composite bead (CSB2) before adsorption and after 24 h adsorption of nickel (CSB2–Ni).

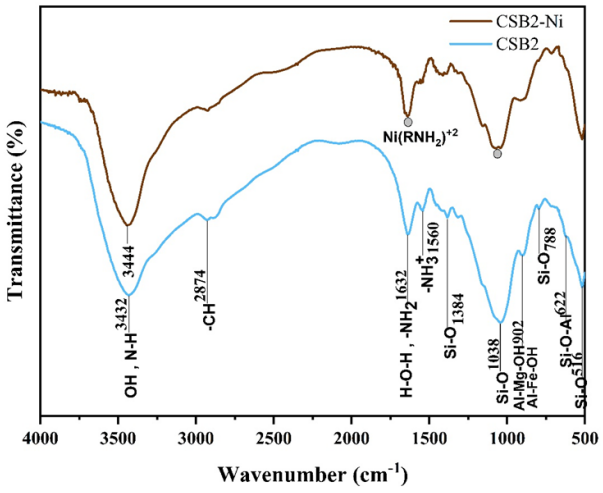

Figure 9. FTIR spectra of the chitosan/bentonite composite bead before adsorption (CSB2) and after 24 h nickel adsorption (CSB2–Ni)

As previously mentioned, in the chitosan/bentonite composite beads, part of the chitosan is intercalated between the montmorillonite layers, while another part is polymerized around the bentonite particles. Therefore, in the composite beads before nickel adsorption, vibrational bands corresponding to both montmorillonite and chitosan are observed. The main vibrational bands of

chitosan are summarized in Table 5 and indicated in Fig. 9.

Upon contact of the nickel-containing solution with the chitosan/bentonite composite bead, nickel cations are adsorbed through three main mechanisms: (1) electrostatic attraction by both composite components, (2) complex formation with chitosan as $Ni(RNH_2)^{2+}$, and (3) cation exchange of Ca^{2+} and Na^{+} in montmorillonite with Ni^{2+}. Adsorption and ion exchange can induce slight disorder in the molecular bonds, resulting in broadening of the FTIR peaks in the composite bead, as observed in the CSB2-Ni spectrum compared to that of CSB2 (Fig. 9). However, the formation of the nickel-chitosan complex leads to the appearance of new vibrations and a reduction in the $–NH_2$ band intensity. In Fig. 9, the $Ni(RNH_2)^{2+}$ complex vibration reduces the intensity of the sharp $–NH_2$ peak at ~1632 cm^{-1}, accompanied by a shoulder corresponding to the $–NH_3^{+}$ vibration at ~1560 cm^{-1}. This indicates a decrease in free amino groups due to their complexation with nickel ions. The $–NH_3^{+}$ groups are formed by the protonation of $–NH_2$ groups upon uptake of H^{+} ions.

Figure 9 also shows that the sharp peak corresponding to the Si–O tetrahedral vibrations at ~1038 cm^{-1} becomes broader. This observation suggests that the proximity of SiO_4 tetrahedra to the intercalated chitosan leads to greater disorder in the tetrahedral layers during nickel adsorption. The main vibrational bands of chitosan are summarized in Table 5.

TABLE 5. lists the main vibrational bands of chitosan (Abu Salem et al., 2025; Ngah et al., 2006; Nicomel et al., 2021)

Wavenumber (cm^{-1})	Vibration type / Assignment
3200–3600	O–H and N–H stretching vibrations
2850	–CH stretching
1600–1661	$–NH_2$ stretching
1607	C=N stretching
1545	C=O stretching
1433	CH–OH bending
1342	N–H bending
1213	C–N stretching
1123–1163	C–O and C–H stretching
1030–1103	C–O stretching
603	C=O bending
1632	N–H coordinatewith Ni^{2+}, corresponding to $Ni(RNH_2)^{2+}$ complex formation

3.5. SEM analysis of the bead microstructure

To demonstrate the adsorption of nickel by the prepared chitosan and chitosan/bentonite composite beads, elemental surface analysis was performed on the chitosan beads (CS) after adsorption, and the results are presented in Fig. 10. Similarly, elemental surface analysis was carried out on the chitosan/bentonite composite beads (CSB2) after adsorption, and the corresponding results are shown in Fig. 11. As can be observed, a considerable amount of nickel was clearly detected on the surface, confirming significant adsorption.

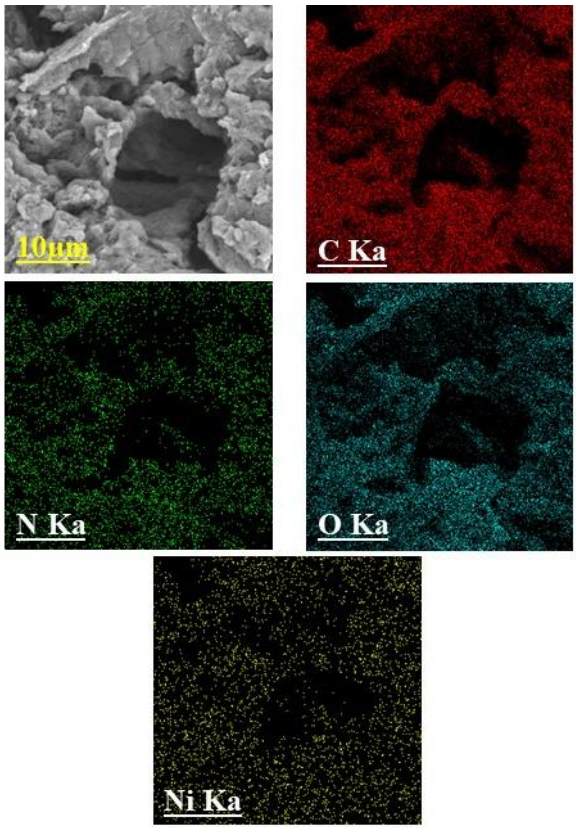

Figure 10. Elemental analysis of the entire surface of chitosan beads after nickel adsorption

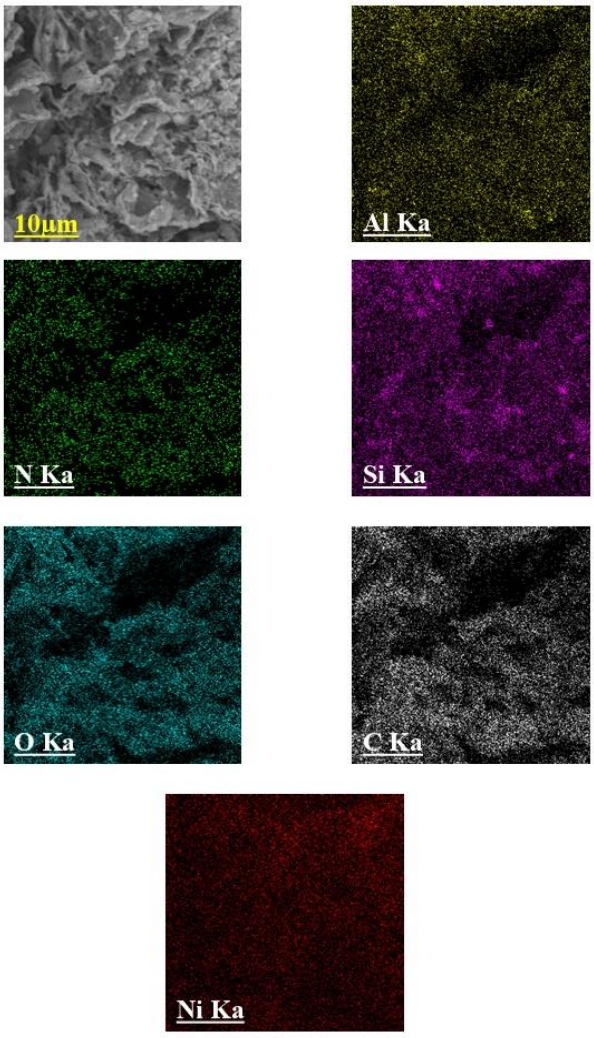

Figure 11. Elemental analysis of the entire surface of the chitosan/bentonite composite after nickel adsorption

3.6. Adsorption isotherms

After determining the equilibrium concentrations in the adsorption experiments using the chitosan/bentonite composite beads, the experimental results were compared with the Langmuir, Freundlich, and Temkin isotherm models to evaluate the fit of the adsorption data, determine the model parameters, and compare them with those of other adsorbents.

The Langmuir model for the thermally activated chitosan/bentonite composite (CSB2) is plotted in Fig. 12. This model is based on homogeneous, monolayer adsorption of atoms or ions onto the active sites of the adsorbent. As shown in Fig. 12, the Langmuir model does not fit the experimental data well, since the adsorption sites of the chitosan/bentonite composite beads do not possess identical chemical potentials.

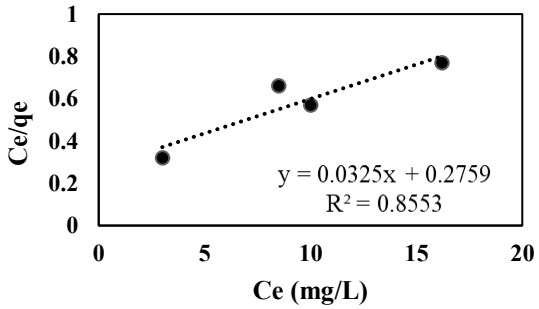

Figure 12. Langmuir isotherm model for nickel cation adsorption by the chitosan/bentonite composite bead (CSB2)

The adsorption results of nickel cations by the chitosan/bentonite composite beads were also analyzed using the Freundlich model, as shown in Fig. 13.

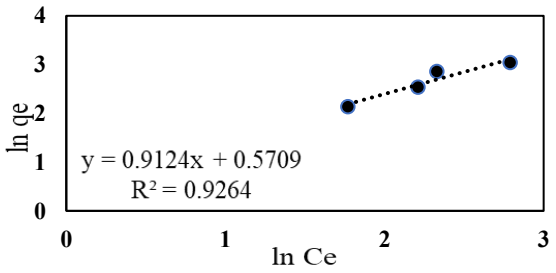

Figure 13. Freundlich isotherm for nickel adsorption by the chitosan/bentonite composite bead (CSB2)

As shown in Fig. 13, the experimental results fit the Freundlich model well. In this model, the adsorbent surface is heterogeneous, meaning that adsorption sites have different activity levels. Adsorption begins at the most active sites and can proceed in multiple layers (Zia et al., 2019). The parameters obtained from this model are summarized in Table 6.

TABLE 6. Freundlich parameters for chitosan/bentonite composite beads

Reference	R^2	1/n (L/mg)	Kf (mg/L)	Sample
This study	0.926	0.909	1.77	Thermally activated chitosan/bentonite bead (CSB2)
[Tsai et al., 2016]	0.972	0.363	-	Chitosan/bentonite composite

Here, Kf represents the relative adsorption capacity, and n indicates the adsorption intensity. If $1/n < 1$, adsorption is predominantly chemical; if $1/n > 1$, adsorption is predominantly physical (de Queiroz Antonino et al., 2017; Román-Doval et al., 2023). Therefore, the values obtained for CSB2 indicate that chemical adsorption, i.e., the formation of $Ni(RNH_2)^{2+}$

complexes at active sites, is more significant than physical adsorption via electrostatic interactions by chitosan and montmorillonite, as well as cation exchange of Ni^{2+} with Na^{+} and Ca^{2+} in montmorillonite.

The comparative data presented in Table 7 clearly indicate that the chitosan/bentonite composite (CSB2) exhibits remarkable adsorption performance for Ni(II) ions. The maximum adsorption capacity obtained in this study is not only comparable to, but in some cases exceeds, those of various chitosan-based adsorbents reported in the literature. These findings highlight the potential of CSB2 as an efficient and cost-effective adsorbent for the treatment of nickel-contaminated wastewater.

TABLE 7. Comparison of maximum adsorption capacities of various chitosan/bentonite-based adsorbents for Ni(II) removal from aqueous solutions.

Reference	C_0(ppm)	Equilibrium adsorption capacity, qe (mg/g)	Adsorbent type
This study	80	18.42	Thermally activated chitosan/bentonite bead
[Tsai et al., 2016]	100	12.4	Chitosan/bentonite composite
[Ibarra-Buscano et al., 2009]	100	11.5	Chitosan/Montmorillonite Beads

The Temkin model was also applied to evaluate nickel adsorption by the CSB2 composite bead, as shown in Fig. 14.

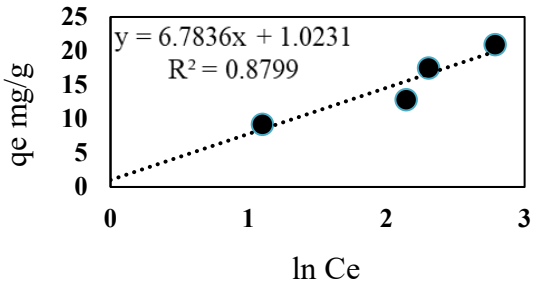

Figure 14. Temkin isotherm for nickel adsorption by chitosan/bentonite composite beads (CSB2)

The Temkin model is based on the interaction between the adsorbate and adsorbent, assuming that the heat of adsorption of the adsorbate in the adsorbed layer decreases linearly with increasing layer thickness. In this model, A represents the Temkin equilibrium constant, and B is a constant related to the adsorption heat, from which the Temkin constant bT (J/mol) can be obtained. Higher values of A indicate greater adsorption capacity, while higher bT values indicate stronger adsorbent–adsorbate interactions. For the CSB2 composite bead, A = 758.5 L/g and bT = 2421.8 J/mol were determined. Ultimately, the Freundlich isotherm exhibited a higher correlation coefficient than the Langmuir and Temkin models, demonstrating better consistency with the experimental findings.

3.7. Adsorption Kinetics

To investigate the adsorption mechanism of nickel ions onto chitosan/bentonite composite beads and to identify the rate-controlling step, the experimental time-dependent data were fitted using three common kinetic models, namely the pseudo-first-order (PFO), pseudo-second-order (PSO), and intra-particle diffusion (IPD) models. The fitting results for these models are presented in Figs. 15, 16, and 17, respectively.

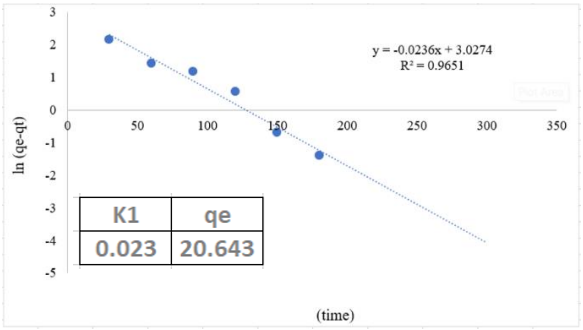

Figure 15. Linear fitting of pseudo-first-order model for adsorption of Ni(II) ions onto chitosan/bentonite composite (CSB2) at initial concentration of 80 mg/L, pH = 7–8, temperature of 25 °C, stirring speed of 200 rpm, and adsorbent dosage of 0.2 g.

As shown in Figure 7 and Table X, the pseudo-first-order model exhibited a correlation coefficient (R^2) of 0.9651, with a calculated equilibrium adsorption capacity (q_e,cal) of 20.643 mg/g and a rate constant (k_1) of 0.023 min^{-1}. Although the R^2 value indicates a relatively acceptable fit, comparison of q_e,cal (20.643 mg/g) with q_e,exp (obtained experimentally) reveals a significant discrepancy, suggesting that the pseudo-first-order model does not adequately describe the adsorption kinetics of Ni(II) onto the chitosan/bentonite composite.

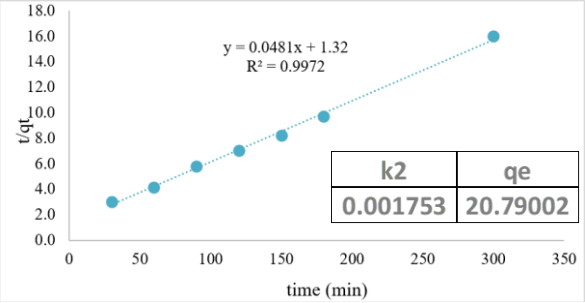

Figure 16. Pseudo-second-order kinetic plot for Ni(II) adsorption onto chitosan/bentonite composite beads (C_0 = 80 mg/L, pH = 7–8, T = 25 °C, adsorbent dosage = 0.2 g, stirring rate = 200 rpm).

As shown in Figure 16 and Table X, the pseudo-second-order model exhibited a high correlation coefficient (R^2 = 0.9972), indicating an excellent fit to the experimental data. The calculated equilibrium adsorption capacity (q_e,cal = 20.790 mg/g) was in close agreement with the experimental value (q_e,exp = ... mg/g), further confirming the suitability of this model. The rate constant (k_2 = 0.001753 g/mg·min) was obtained from the slope and intercept of the linear plot of t/q_t versus t. These results confirm that the pseudo-second-order model provides the best description of Ni(II) adsorption kinetics onto the chitosan/bentonite composite, suggesting that chemisorption is the rate-limiting step. Compared to the pseudo-first-order model (R^2 = 0.9651, q_e,cal = 20.643 mg/g), the pseudo-second-order model showed superior performance, confirming its reliability for describing the adsorption kinetics.

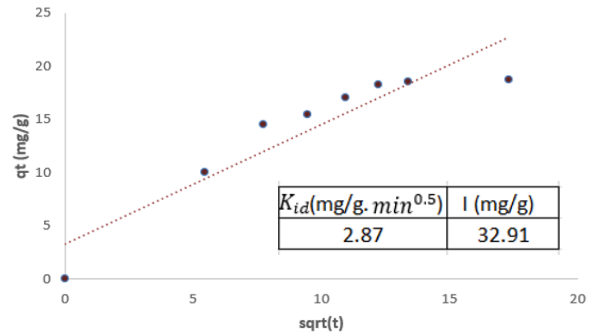

Figure 17. Intra-particle diffusion plot for Ni(II) adsorption onto chitosan/bentonite composite beads (C_0 = 80 mg/L, pH = 7–8, T = 25 °C, adsorbent dosage = 0.2 g, stirring rate = 200 rpm).

As shown in Figure 17, the intra-particle diffusion model exhibited a correlation coefficient (R^2) of 0.798, with a diffusion rate constant (k_i) of 2.87 mg/g·$min^{0.5}$ and an intercept (C) of 32.91 mg/g. The relatively low R^2 value compared to that of the pseudo-second-order model (0.9972) indicates that intra-particle diffusion alone cannot adequately describe the adsorption kinetics. Furthermore, the linear plot does not pass through the origin ($C \neq 0$), confirming that intra-particle diffusion is not the sole rate-controlling mechanism. The high value of C (32.91 mg/g) suggests that film diffusion (mass transfer from the bulk solution to the adsorbent surface) also plays a significant role in the overall adsorption process. Therefore, the adsorption of Ni(II) ions onto the chitosan/bentonite composite is controlled by a combination of both film diffusion and intra-particle diffusion mechanisms.

In conclusion, the pseudo-second-order model provides the best description of the Ni(II) adsorption kinetics onto the chitosan/bentonite composite, indicating that chemisorption is the dominant rate-controlling mechanism. However, the contributions of both film diffusion and intra-particle diffusion to the overall adsorption process should also be considered.

4. CONCLUSION(S)

- Chitosan/bentonite composite beads were prepared by mixing a suspension containing 0.75 g of Iranian bentonite in 100 mL of water with 1.5 g of medium-molecular-weight chitosan dissolved in 100 mL of a 2% aqueous acetic acid solution for 4 h, followed by dropwise addition into an alkaline solution containing NaOH at pH 7-8 and curing for 24 h, resulting in beads approximately 3 mm in diameter.
- During thermal activation of bentonite at 400 °C for 3 h, only the molecular water between the montmorillonite layers was removed, while the OH groups of the octahedral sheets, which play a key role in pollutant adsorption, remained intact. The removal of interlayer water reduced the basal spacing (001) of montmorillonite from 13.4 Å to 10.72 Å.
- The percentage removal and equilibrium adsorption capacity of Ni^{2+} at an initial concentration of 80 ppm by chitosan beads were 84.5% and 16.9 mg/g, respectively. For the chitosan/bentonite composite bead with a chitosan-to-bentonite weight ratio of 2:1, these values increased to 90.4% and 18.42 mg/g, corresponding to relative increases of 6.9% and 8.9%, respectively.
- The effect of pH on the adsorption of Ni^{2+} (80 ppm) showed that the maximum adsorption by CSB2 composite beads occurred at pH 7.5, achieving 90.4%.
- Fourier-transform infrared spectroscopy (FTIR) analysis of the composite beads revealed that, after Ni^{2+} adsorption, $Ni(RNH_2)^{2+}$ complexes were clearly formed at 1632 cm^{-1}, which also induced structural disorder in the montmorillonite layers.
- Among the adsorption isotherm models tested, namely Langmuir, Freundlich, and Temkin, the Langmuir model did not fit the experimental data well. The Freundlich model parameters were Kf = 1.77 mg/L and 1/n = 0.909, while the Temkin parameters were A = 0.33 L/mg and bT = 195.6 J/mol.

ACKNOWLEDGEMENTS

The authors gratefully acknowledge the technical support provided by the central laboratory of Iran University of Science and Technology (IUST) for the characterization analyses (SEM, FTIR, XRD, and DTA/TG). We also thank our research group members for their valuable assistance.

REFERENCES

1. Abu Salem, H. S., Hassan, S. S., Refay, F. A., Sulieman, Z. K., Mohamed, M. Y., Rabea, A. R.,…Mohamed, F. M. (2025). Modified bentonite @ microwave for Mn(VII) removal with a simulation study. *Scientific Reports*, *15*(1), 8520. https://doi.org/10.1038/s41598-025-91906-z

2. Ahmad, L. O., Permana, D., Wahab, Sabarwati, S., Ramadhan, L. O. A., & Rianse, U. (2015). *Improved Chitosan Production from Tiger Shrimp Shell Waste (Penaeus monodon) by Multistage Deacetylation Method and Effect of Bleaching*. (https://api.semanticscholar.org/CorpusID:171084048)

3. Al-Nuaim, M. A., Alwasiti, A. A., & Shnain, Z. Y. (2023). The photocatalytic process in the treatment of polluted water. *Chemical papers*, *77*(2), 677-701. https://doi.org/10.1007/s11696-022-02468-7

4. Alemu, D., Getachew, E., & Mondal, A. K. (2023). Study on the Physicochemical Properties of Chitosan and their Applications in the Biomedical Sector. *International Journal of Polymer Science*, *2023*(1), 5025341. https://doi.org/10.1155/2023/5025341

5. Aliku, O. (2017). Desalination: A Means of Increasing Irrigation Water Sources for Sustainable Crop Production. In. https://doi.org/10.5772/intechopen.69312

6. Bahranowski, K., Klimek, A., Gaweł, A., & Serwicka, E. M. (2021). Rehydration driven Na-activation of bentonite evolution of the clay structure and composition. *Materials*, *14*(24), 7622. https://doi.org/10.3390/ma14247622

7. Buscano, S., Lourdes, M., Dalida, P., Wan, M.-W., & Kan, C.-C. (2009). *Chitosan-Montmorillionite Composite Beads as Adsorbents for Heavy Metals Uptake from Aqueous Medium*. (https://www.researchgate.net/publication/282156668)

8. Dada, A., Olalekan, A., Olatunya, A., & Dada, O. (2012). Langmuir, Freundlich, Temkin and Dubinin–Radushkevich Isotherms Studies of Equilibrium Sorption of Zn 2+ Unto Phosphoric Acid Modified Rice Husk. *J. Appl. Chem.*, *3*, 38-45. https://doi.org/10.9790/5736-0313845

9. de Queiroz Antonino, R. S. C. M., Lia Fook, B. R. P., de Oliveira Lima, V. A., de Farias Rached, R. Í., Lima, E. P. N., da Silva Lima, R. J.,…Lia Fook, M. V. (2017). Preparation and characterization of chitosan obtained from shells of shrimp (Litopenaeus vannamei Boone). *Marine drugs*, *15*(5), 141. https://doi.org/0.3390/md15050141

10. do Nascimento, G. M. (2021). Introductory Chapter: Polymers and Clays-A Fruitful Combination. *Clay and Clay Minerals*, 3. https://doi.org/10.5772/intechopen.101296

11. El-Baz, A. A. A., Hendy, I. A., Dohdoh, A. M., & Srour, M. I. (2020). Adsorption technique for pollutants removal; current new trends and future challenges–A Review. *The Egyptian International Journal of Engineering Sciences and Technology*, *32*(Civil and Architectural Engineering), 1-24. https://doi.org/10.21608/eijest.2020.45536.1015

12. Eser, A., Tirtom, V. N., Aydemir, T., Becerik, S., & Dinçer, A. (2012). Removal of nickel (II) ions by histidine modified chitosan beads. *Chemical Engineering Journal*, *210*, 590-596. https://doi.org/10.1016/j.cej.2012.09.020

13. Giannakas, A., & Pissanou, M. (2018). Chitosan/bentonite nanocomposites for wastewater treatment: a review. *SF J Nanochem Nanotechnol. 2018; 1 (1), 1010*. (https://www.researchgate.net/publication/329311716)

14. Guibal, E. (2004). Interactions of metal ions with chitosan-based sorbents: a review. *Separation and Purification Technology*, *38*(1), 43-74. https://doi.org/10.1016/j.seppur.2003.10.004

15. Gupta, A., Sharma, V., Sharma, K., Kumar, V., Choudhary, S., Mankotia, P.,…Ekielski, A. (2021). A review of adsorbents for heavy metal decontamination: Growing approach to wastewater treatment. *Materials*, *14*(16), 4702. https://doi.org/10.3390/ma14164702

16. Hodžić, N., Đozić, A., Šestan, I., & Alihodžić, H. (2020). Examination of Adsorption Abilities of Natural and Acid Activated Bentonite for Heavy Metals Removal from Aqueous Solutions. *International Journal for Research in Applied Sciences and Biotechnology*, *7*(1). https://doi.org/10.31033/ijrasb.7.1.1

17. Institute of Standards and Industrial Research of Iran. (1990). (https://www.scribd.com/document/733977992/Institute-of-Standards-and-Industrial-Research-of-Iran)

18. Jozanikohan, G., & Abarghooei, M. N. (2022). The Fourier transform infrared spectroscopy (FTIR) analysis for the clay mineralogy studies in a clastic reservoir. *Journal of Petroleum Exploration and Production Technology*, *12*(8), 2093-2106. https://doi.org/10.1007/s13202-021-01449-y

19. Madejova, J. (2003). FTIR techniques in clay mineral studies. *Vibrational Spectroscopy*, *31*, 1-10. https://doi.org/10.1016/S0924-2031(02)00065-6

20. Majiya, H., Clegg, F., & Sammon, C. (2023). Bentonite-Chitosan composites or beads for lead (Pb) adsorption: Design, preparation, and characterisation. *Applied Clay Science*, *246*, 107180. https://doi.org/10.1016/j.clay.2023.107180

21. Ngah, W. W., Kamari, A., Fatinathan, S., & Ng, P. (2006). Adsorption of chromium from aqueous solution using chitosan beads. *Adsorption*, *12*, 249-257. https://doi.org/10.1007/s10450-006-0501-0

22. Nicomel, N. R., Otero-Gonzalez, L., Folens, K., Mees, B., Hennebel, T., & Du Laing, G. (2021). Selective and enhanced nickel adsorption from sulfate- and calcium-rich solutions using chitosan. *Separation and Purification Technology*, *276*, 119283. https://doi.org/10.1016/j.seppur.2021.119283

23. Pirilä, M. (2015). Adsorption and photocatalysis in water treatment: active, abundant and inexpensive materials and methods. (https://urn.fi/URN:ISBN:9789526207629)

24. Román-Doval, R., Torres-Arellanes, S. P., Tenorio-Barajas, A. Y., Gómez-Sánchez, A., & Valencia-Lazcano, A. A. (2023). Chitosan: Properties and its application in agriculture in context of molecular weight. *Polymers*, *15*(13), 2867. https://doi.org/10.3390/polym15132867

25. Salimi, M., Arifin, Y. F., & Ansari, M. (2025). shear strength and permeability of bentonite–chitosan composites with naturally graded sands. *GEOMATE Journal*, *28*(129), 66-75. (https://geomatejournal.com/geomate/article/view/4865)

26. Teofilović, V., Pavličević, J., Bera, O., Jovičić, M., Budinski-Simendić, J., Mészáros-Szécsényi, K., & Aroguz, A. (2014). Preparation and thermal properties of chitosan/bentonite composite beads. *Hemijska industrija*, *68*(6), 653-659. https://doi.org/10.2298/HEMIND130905088T

27. Tirtom, V. N., Dinçer, A., Becerik, S., Aydemir, T., & Çelik, A. (2012). Comparative adsorption of Ni(II) and Cd(II) ions on epichlorohydrin crosslinked chitosan–clay composite beads in aqueous solution. *Chemical Engineering Journal*, *197*, 379-386. https://doi.org/10.1016/j.cej.2012.05.059

28. Vijaya, Y., Popuri, S. R., Boddu, V. M., & Krishnaiah, A. (2008). Modified chitosan and calcium alginate biopolymer sorbents for removal of nickel (II) through adsorption. *Carbohydrate polymers*, *72*(2), 261-271. https://doi.org/10.1016/j.carbpol.2007.08.010

29. Wang, H., Shirakawabe, T., Komine, H., Ito, D., Gotoh, T., Ichikawa, Y., & Chen, Q. (2019). Movement of water in compacted bentonite and its relation with swelling pressure. *Canadian Geotechnical Journal*, *57*(6), 921-932. https://doi.org/10.1139/cgj-2019-0219

30. Wang, J., & Chen, C. (2014). Chitosan-based biosorbents: Modification and application for biosorption of heavy metals and radionuclides. *Bioresource Technology*, *160*, 129-141. https://doi.org/10.1016/j.biortech.2013.12.110

31. Zhu, R., Chen, Q., Zhou, Q., Xi, Y., Zhu, J., & He, H. (2016). Adsorbents based on montmorillonite for contaminant removal from water: A review. *Applied Clay Science*, *123*, 239-258. https://doi.org/10.1016/j.clay.2015.12.024

32. Zia, Q., Tabassum, M., Gong, R., & Li, J. (2019). A Review on Chitosan for the Removal of Heavy Metals Ions. *Journal of Fiber Bioengineering and Informatics*, *12*, 103-128. https://doi.org/10.3993/jfbim00301